Acta Crystallographica Section D
Biological Crystallography
ISSN 0907-4449

Structure of xylanase Xys1Δ from *Streptomyces halstedii*

Albert Canals,[a]* M. Cristina Vega,[a] F. Xavier Gomis-Rüth,[a] Margarita Díaz,[b] Ramón I. Santamaría[b] and Miquel Coll[a]

[a]Institut de Biologia Molecular de Barcelona, Consejo Superior de Investigaciones Científicas, Jordi Girona 18–26, 08034 Barcelona, Spain, and [b]Instituto de Microbiología Bioquímica, Departamento de Microbiología y Genética, Consejo Superior de Investigaciones Científicas/Universidad de Salamanca, Salamanca, Spain

Correspondence e-mail: acpcri@ibmb.csic.es

Received 8 May 2003
Accepted 6 June 2003

PDB Reference: Xys1Δ, 1nq6, r1nq6sf.

Xylanases hydrolyze the β-1,4-linked xylose backbone of xylans. They are of increasing interest in the paper and food industries for their pre-bleaching and bio-pulping applications. Such industries demand new xylanases to cover a wider range of cleavage specificity, activity and stability. The catalytic domain of xylanase Xys1 from *Streptomyces halstedii* JM8 was expressed, purified and crystallized and native data were collected to 1.78 Å resolution with an $R_{\rm merge}$ of 4.4%. The crystals belong to space group $P2_12_12_1$, with unit-cell parameters a = 34.05, b = 79.60, c = 87.80 Å. The structure was solved by the molecular-replacement method using the structure of the homologue Xyl10A from *Streptomyces lividans*. In a similar manner to other members of its family, Xys1 folds to form a standard $(\beta/\alpha)_8$ barrel with the two catalytic functions, the acid/base and the nucleophile, at its C-terminal side. The overall structure is described and compared with those of related xylanases.

1. Introduction

Endoxylanases (1,4-β-D-xylanohydrolases; EC 3.2.1.8) catalyze the hydrolysis of the internal β-xylosidic glycosidic bonds of xylan, the major component of hemicellulose in plant cell walls, and are produced by several microorganisms. Xylanases have many applications in the pharmaceutical and food industries and enable a nature-friendly biobleaching process in paper production. These industries demand enzymes with increased stability and activity and with the ability to degrade the variety of glycosidic bonds found in xylan.

Most xylanases fall into families 10 and 11 of the sequence-based classification of glycoside hydrolases (Henrissat, 1991; Henrissat & Bairoch, 1993, 1996). Family 10 xylanases are modular enzymes, usually with a catalytic domain (CD) and a carbohydrate-binding domain, normally a cellulose-binding domain (CBD) or a xylan-binding domain (XBD), connected to the CD by a flexible linker. The CDs of these xylanases typically adopt a $(\beta/\alpha)_8$ TIM-barrel-type fold (Banner *et al.*, 1975). The crystal structure of a full-length xylanase from this family, FXYN from *Streptomyces olivaceoviridis* E-86 (Fujimoto *et al.*, 2000), has been reported. High-resolution X-ray structures are available for the CDs of XYLA from *Pseudomonas fluorescens* (Harris *et al.*, 1994, 1996), Cex from *Cellulomonas fimi* (White *et al.*, 1994) and Xyl10A from *S. lividans* (Derewenda *et al.*, 1994; Ducros *et al.*, 2000), *Clostridium thermocellum* (Domínguez *et al.*, 1995), *Penicillium simplicissimum* (Schmidt *et al.*, 1998) and *Thermoascus aurantiacus* (Natesh *et al.*, 1999, 2003). Structures of the complexes of some of these enzymes with diverse substrates are also

available. The structural analyses of trapped covalent intermediates in the CDs of Cex from *C. fimi* (White *et al.*, 1996; Notenboom *et al.*, 1998) and Xyl10A from *S. lividans* (Ducros *et al.*, 2000) have provided valuable information on the catalytic mechanism. Two glutamate residues are considered to be the catalytic residues, one acting as a proton donor and the other as a nucleophilic base in a double-displacement mechanism (Henrissat & Davies, 1997).

Two forms of the family 10 xylanase Xys1 from the actinomycete *S. halstedii* JM8, namely Xys1L and Xys1S, occur naturally as a result of the expression of a single gene, *xysA* (Ruiz-Arribas *et al.*, 1997; GenBank accession No. U41627). Xys1S (33.7 kDa) is the proteolyzed form of full-length Xys1L (45 kDa) and comprises only the CD and a Gly-rich C-terminal linker (Fig. 1). Whereas Xys1L is likely to hydrolyze insoluble xylan and complex hemicellulose substrates, rendering short soluble oligosacharides, the Xys1S form (lacking the CBD) is probably more useful, hydrolyzing these soluble fragments of xylan. Both forms have been isolated, cloned, overexpressed, purified and characterized (Ruiz-Arribas *et al.*, 1995, 1997, 1998). Although neither Xys1L nor Xys1S formed crystals, the crystallization of the CD was accomplished with a variant called Xys1Δ obtained by removing the Gly-rich region of Xys1S (Ruiz-Arribas *et al.*, 1998). In this paper, we report the crystal structure determination of Xys1Δ at 1.78 Å resolution and compare it with closely related structures.

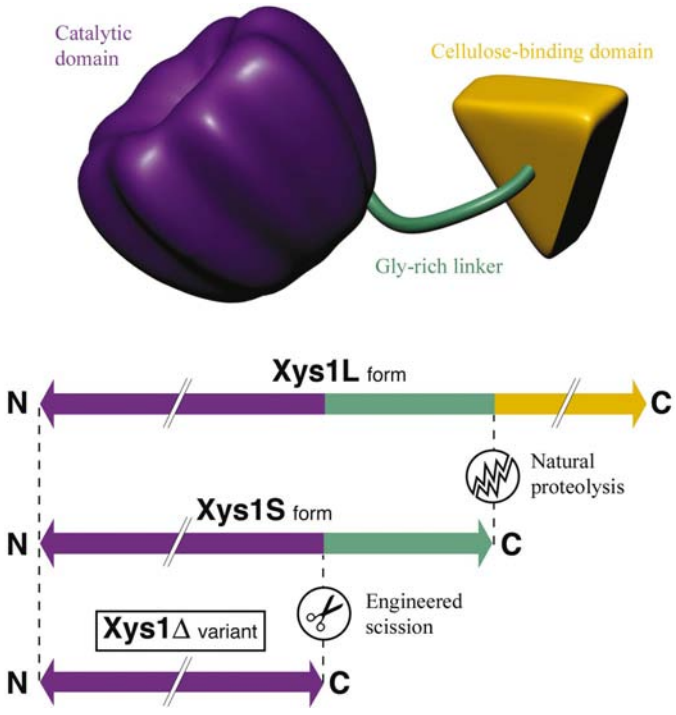

Figure 1
Diagram of full-length xylanase Xys1L from *S. halstedii* showing its two domains and linker. Natural proteolysis of the cellulose-binding domain yields Xys1S. Engineered removal of both the cellulose-binding domain and the Gly-rich linker allowed the crystallization of the catalytic domain, the variant called Xys1Δ. The N-terminal residue of these three proteins corresponds to residue 46 of the ORF.

2. Materials and methods

2.1. Crystallization and data collection

Xylanases Xys1L, Xys1S and their truncated form Xys1Δ were cloned, expressed in *S. lividans* 66 and purified according to the previously described procedures (Ruiz-Arribas *et al.*, 1995, 1998). Attempts to crystallize the enzyme were unfruitful until both the cellulose-binding domain and the glycine-rich tail regions were removed from the gene, yielding variant Xys1Δ. The first of the 302 residues composing the mature form of Xys1Δ is actually residue 46 of the original *Streptomyces* open reading frame (ORF), as the first 45 residues correspond to a long signal peptide which is cleaved and lost. Crystallization of Xys1Δ was achieved using the vapour-diffusion technique at room temperature. The crystals grew from hanging drops containing 3 µl of 15 mg ml^{-1} protein and 3 µl of precipitant solution (10% PEG 4000, 0.1 *M* $MgCl_2$ and 0.1 *M* sodium acetate buffer pH 5.5) equilibrated against 500 µl of precipitant solution. Crystals appeared in six weeks with typical dimensions of 1.0 × 0.4 × 0.1 mm. They were washed with harvesting buffer (20% PEG 4000, 0.2 *M* $MgCl_2$ and sodium acetate buffer pH 5.5) and flash-cryocooled under an N_2 steam.

A complete diffraction data set was collected on a MAR 345 image-plate scanner (MAR Research) from a single crystal kept at 120 K using synchrotron radiation (λ = 0.885 Å) at the EMBL beamline BW7B at DESY (Hamburg). The crystal-to-detector distance was 130 mm. The crystal diffracted to 1.78 Å, belongs to space group $P2_12_12_1$ with unit-cell parameters a = 34.05, b = 79.60, c = 87.80 Å and contains one Xys1Δ molecule per asymmetric unit. Data were indexed and integrated with *DENZO* (Otwinowski, 1993) and scaled with *SCALA* (Evans, 1993). The data set has an R_{merge} of 4.4% and a completeness of 97.1% in the resolution range 25–1.78 Å. Data-collection statistics are shown in Table 1.

2.2. Structure determination and refinement

The structure was solved by the molecular-replacement method with *AMoRe* (Navaza, 1994) using the homologue Xyl10A from *S. lividans* (Ducros *et al.*, 2000; PDB code 1e0w) as a search model. Reflections within the resolution range 15–3.5 Å were used for rotation- and translation-function calculations. One clear solution was found with a correlation coefficient of 42.7% and a crystallographic R factor of 45.1% (values for the highest noise peak are 25.6 and 24.1%, respectively).

Initial automatic density-map interpretation and model building was performed with the *warpNtrace* application of *ARP/wARP* (Perrakis *et al.*, 1997). The program identified 298 out of 302 side chains in accordance with the chemical sequence. All data were used (25–1.78 Å) with no low-resolution or σ-cutoff. Water molecules were added with the automatic protocol of *ARP/wARP* and were checked visually for reasonable stereochemistry and goodness of fit to the electron-density maps. Subsequent rounds of structure refinement were carried out alternating *CNS* (Brünger *et al.*, 1998) and manual model building using *TURBO-FRODO*

Table 1
Data-collection and refinement statistics.

Values in parentheses correspond to the highest resolution shell (1.88–1.78 Å).

Data collection	
Space group	$P2_12_12_1$
Unit-cell parameters (Å)	a = 34.05, b = 79.6, c = 87.8
Resolution range (Å)	25–1.78
Completeness (%)	97.1 (85.8)
$\langle I\rangle/\langle\sigma(I)\rangle$	13.1 (8.9)
Average multiplicity	3.4 (2.7)
No. of observed reflections	78251
No. of unique reflections	22905
$R_{\rm merge}$† (%)	4.4 (8.4)
Refinement statistics	
No. of molecules per asymmetric unit	1
Resolution range used for refinement (Å)	25–1.78
No. of reflections in working set	21207
No. of reflections in test set	1658
No. of protein atoms included in refinement	2300
No. of solvent molecules	341
No. of cations	1 (Mg^{2+})
R factor/$R_{\rm free}$‡	0.15/0.18 (0.16/0.22)
R.m.s. deviation from target values	
Bond lengths (Å)	0.009
Bond angles (°)	1.090
Avarage B factors (Å^2)	
Protein, overall	11.9
Main chain	11.4
Side chain	12.4
Water	22.6
Ramachandran statistics§	
No. of outliers	2
Percentage of outliers	0.7

† $R_{\rm merge} = [\sum_{hkl}\sum_i |I_i(hkl) - \langle I(hkl)\rangle|/\sum_{hkl}\sum_i I_i(hkl)] \times 100$, where I_i is the ith measurement of reflection hkl and symmetry-related reflections and $\langle I(hkl)\rangle$ is its mean value. ‡ $R = R_{\rm free} = \sum_{hkl} ||F_{\rm obs} - k|F_{\rm calc}||/\sum_{hkl}|F_{\rm obs}|$ calculated for the reflections of the working and test (7.3%) sets, respectively. § Kleywegt & Jones (1996).

(Roussel & Cambillau, 1989) on σ_A-weighted $2F_o - F_c$ and $F_o - F_c$ Fourier maps. A randomly selected 1658 reflections (7.3%) were set aside for $R_{\rm free}$ calculations. Bulk-solvent correction was applied. In the final cycles of refinement, alternate conformations were built for the side chains of residues 57 and 68 and for the disulfide bond between residues 169 and 200. A magnesium ion was assigned on the basis of the electron density, the octahedral coordination sphere and ligand distances. A final refinement cycle was performed with *REFMAC*5 (Murshudov *et al.*, 1999), applying ten cycles of TLS refinement with two TLS chains (one for the protein and one for the solvent molecules). The final model has an R factor of 0.148 and an $R_{\rm free}$ of 0.176. Refinement statistics are shown in Table 1.

The final structure was validated with *PROCHECK* (Laskowski *et al.*, 1993). The Ramachandran plot (Ramachandran & Sasisekharan, 1968) shows that 91.7% of the non-glycine and non-proline residues in the asymmetric unit are located in the most favoured regions, 7.9% are in additional allowed regions and only one residue (0.4%) is in a generously allowed region. None of the residues are located in a disallowed region. There are only two outliers (0.7%) in the more stringent Ramachandran plot devised by Kleywegt & Jones (1996). The model has excellent stereochemical quality, with r.m.s. deviations from ideal values being 0.009 Å for bond lengths and 1.09° for bond angles. The mean protein temperature factor calculated after TLS refinement is 11.9 Å^2.

A least-squares superimposition of the final model of Xys1Δ with those of related xylanases was performed with *TURBO-FRODO* (Roussel & Cambillau, 1989). *B*-factor statistics were calculated with *BAVERAGE* from the *CCP*4 package (Collaborative Computational Project, Number 4, 1994). Figures were generated with *RIBBONS* (Carson, 1997) and *TURBO-FRODO*.

3. Results and discussion

3.1. Overall structure

Only one molecule of Xys1Δ is present per asymmetric unit, with 2300 non-H protein atoms, 341 water molecules and a magnesium ion. Owing to the high quality of the data, only four residues could not be traced automatically using *warpNtrace*. Residues 1 and 2 (slightly disordered), residue 81 (affected by a non-prolyl *cis*-peptide bond) and the

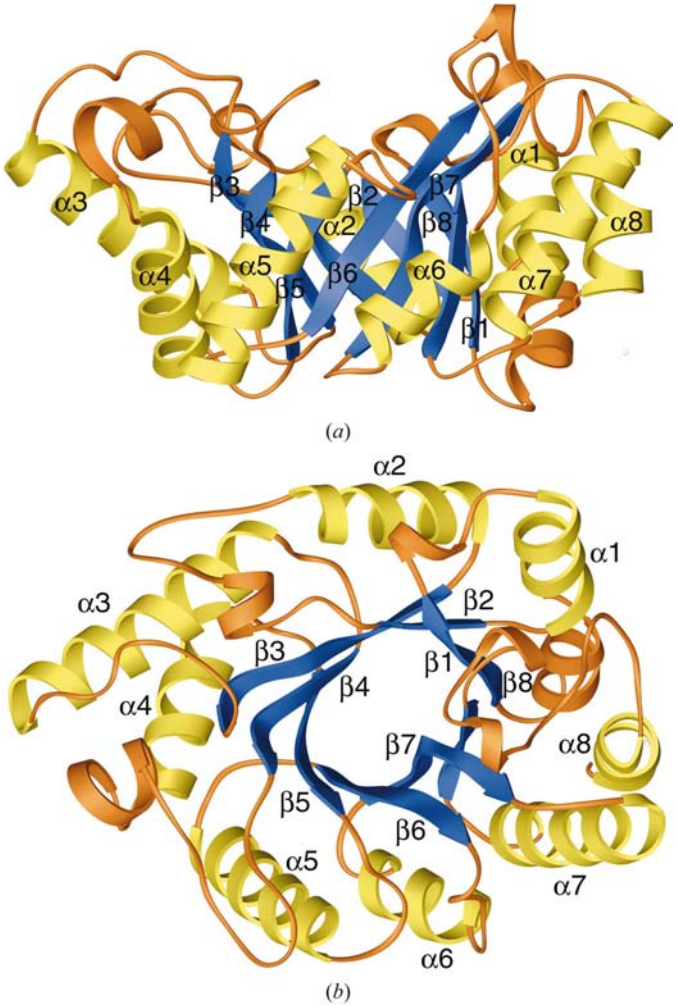

Figure 2
Ribbon representation of Xys1Δ. For clarity, only the major secondary-structure elements forming the $(\beta/\alpha)_8$ barrel have been labelled. Additional minor helices are coloured orange. (*a*) Side view of the catalytic domain, with the carbonyl side of the β-barrel facing upwards. (*b*) Top view of the molecule.

magnesium-coordinating C-terminal residue 302 were traced manually afterwards. The final structure, refined employing data to 1.78 Å resolution, extends from residue 1 to 302 (the entire polypeptide chain) with no breaks in the main-chain density. Side chains are also clearly defined, with only minor disorder at the outermost atoms of some residues (Asp49, Arg65, Gln71, Gln177, Gln193, Lys251, Lys273 and Lys291). Possible alternate conformations were checked for all residues with slightly disordered density. Serine residues 57 and 69 have clear double conformations for their O^{γ} atoms, which are in all cases hydrogen bonded to either water molecules or residues from a neighbouring molecule in the crystal. As discussed later, a further double conformation has been assigned to atom S^{γ} of Cys200.

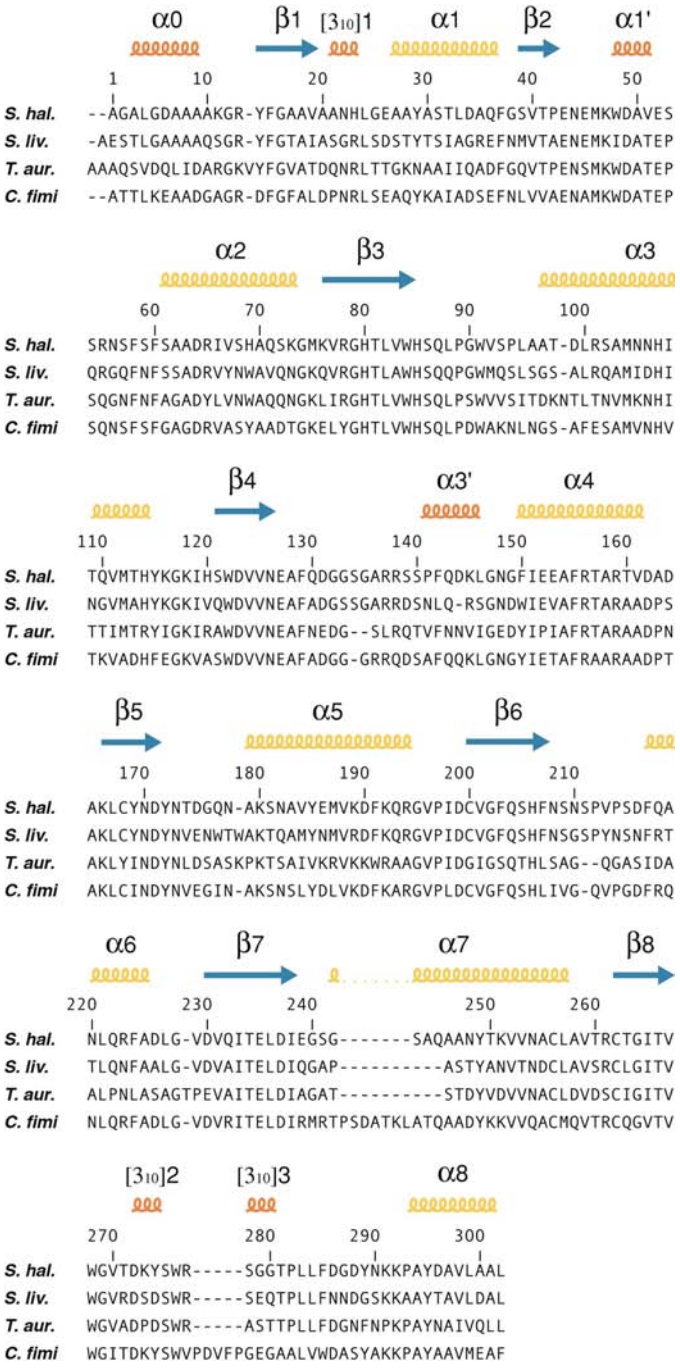

Figure 3
Sequence-based alignment of xylanases from related species (*S. halstedii*, *S. lividans*, *T. aurantiacus* and *C. fimi*), with the secondary-structure elements from Xys1Δ as defined by *DSSP* (Kabsch & Sander, 1983). β-Barrel strands (blue): $\beta1$ (residues 14–19), $\beta2$ (residues 39–42), $\beta3$ (residues 76–84), $\beta4$ (residues 121–126), $\beta5$ (residues 166–171), $\beta6$ (residues 200–203/206–207), $\beta7$ (residues 230–238) and $\beta8$ (residues 262–267). Outer-barrel helices (yellow): $\alpha1$ (residues 27–36), $\alpha2$ (residues 61–73), $\alpha3$ (residues 97–114), $\alpha4$ (residues 150–161), $\alpha5$ (residues 179–194), $\alpha6$ (residues 217–225), $\alpha7$ (residues 242–257), $\alpha8$ (residues 293–301). Minor helices (orange): $\alpha0$ (residues 3–9), $\alpha1'$ (residues 48–51), $\alpha3'$ (residues 141–146), [3$_{10}$]1 (residues 21–23), [3$_{10}$]2 (residues 272–274) and [3$_{10}$]3 (residues 278–280).

Xys1Δ folds in an $(\alpha/\beta)_8$ barrel. Eight parallel twisted β-strands ($\beta1$–$\beta8$) are surrounded by eight major α-helices ($\alpha1$–$\alpha8$) in a right-handed β–α–β motif (Fig. 2). Long $\beta\alpha$ loops at the carbonyl side of the β-barrel (top face in Fig. 2*a*) confer a larger radius to the face where the active site is located and give a 'salad-bowl' shape to the molecule. Cross-sections are quite elliptical at the C-terminal side of the barrel, with maximum shorter and longer axes of ∼40 and ∼55 Å, respectively. The amino side (bottom face in Fig. 2*a*) is rounder, with a diameter of ∼35 Å. The height of the barrel is ∼30 Å. Helix $\alpha1$ is, in fact, composed of a 3$_{10}$-helix (residues 21–23) and a β-turn followed by an α-helix (residues 27–36), as in other members of the family 10 xylanases. Shorter α-helices appear at the N-terminal end ($\alpha0$, residues 3–9) and after strands $\beta2$ ($\alpha1'$, residues 48–51) and $\beta4$ ($\alpha3'$, residues 141–146). Two 3$_{10}$-helices in loop $\beta8\alpha8$ (residues 272–274 and residues 278–280) complete the helical content of the catalytic core (see Fig. 3 for secondary-structure element definitions). There are two disulfide bonds, Cys168–Cys200 and Cys256–Cys262, another conserved feature within family 10.

3.2. Active-site structure

The catalytic activity of all known xylanases is based on a double-displacement mechanism for the hydrolysis of the xylosidic bond. In family 10 xylanases two conserved glutamic acid residues take part in this double-displacement mechanism, one acting as a nucleophile and the other one as a general acid, at the carboxyl (wider) side of the barrel. In Xys1 from *S. halstedii*, Glu235 (in strand $\beta7$) plays the role of the nucleophile, while Glu127 (in loop $\beta4\alpha4$) is the acid/base catalyst (Fig. 4*a*). Their two C^{α} and carboxylate carbon (C^{δ}) atoms are 12.7 and 7 Å apart, respectively. The side chain of Glu235 takes part in two hydrogen bonds, one between its $O^{\varepsilon1}$ atom and His206 $N^{\varepsilon2}$, and one between its $O^{\varepsilon2}$ atom and Asn170 $N^{\delta2}$. The hydrogen bond with His206 may be necessary to maintain the ionized state of the nucleophile Glu235, as has been suggested for the equivalent residues in Xyl10A from *S. lividans* (Roberge *et al.*, 1997). Glu127 is hydrogen bonded to Trp84 (Glu127 $O^{\varepsilon1}$ and Trp84 $N^{\varepsilon1}$) and Gln204 (Glu127 $O^{\varepsilon2}$ and Gln204$N^{\varepsilon2}$). An aromatic cage made by Trp84, Trp268 and Trp276 surrounds the catalytic pocket. Two water molecules inside this pocket, Wat173 and Wat256, are only 2.18 Å apart. In spite of such a close contact, we decided to assign two solvent molecules to the electron densities, as

both persisted after any attempt to move or remove one of the molecules.

3.3. Remarkable structural features

Thr81 is one of the residues that could not be traced automatically. The reason for this is the *cis* conformation of the peptide bond between His80 and Thr81 (Fig. 4*b*). This peculiar non-prolyl *cis*-peptide has been previously described in the structure of xylanase Cex from *C. fimi* (White *et al.*, 1994; PDB code 2exo). It was also reported in the structure of the trapped 2-F xylobiosyl enzyme intermediate of Xyl10A from *S. lividans* (Ducros *et al.*, 2000; PDB code 1e0x). These structures, together with site-directed mutagenesis (Roberge *et al.*, 1997), confirm that His80 has to adopt such a conformation in order to coordinate the O(3) hydroxyl atom of a sugar substrate at subsite −1 (Ducros *et al.*, 2000).

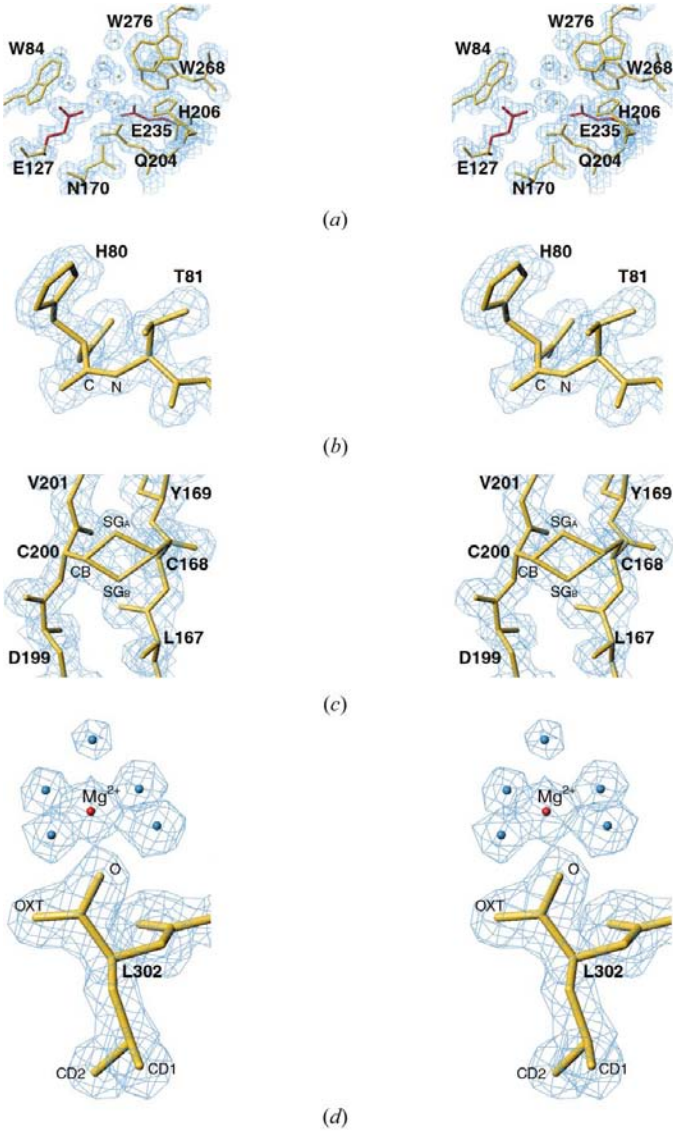

Figure 4
Stereoviews of four structural details in the Xys1Δ structure. (*a*) Active site of the enzyme, with the two catalytic glutamic acid residues coloured red. (*b*) Conserved *cis*-peptide bond between His80 and Thr81. (*c*) Double conformation at the Cys168–Cys200 disulfide bond. (*d*) Magnesium-coordinating Leu302 at the C-terminal end of the polypeptide chain. The $2F_o - F_c$ electron-density maps are contoured at the 1.0σ level.

Another outstanding observation is the alternate conformation of the disulfide bond between Cys168 and Cys200 (Fig. 4*c*). Among xylanases, this feature has been reported only for Xyl10A from *S. lividans*, in a structure that was refined with data to 1.2 Å resolution (Ducros *et al.*, 2000; PDB code 1e0w). The two alternative positions for atom S^{γ} from Cys200 were refined for their occupancies, resulting in 66 and 33%, respectively. This configuration gave a featureless profile in $F_o - F_c$ density maps and balanced the *B*-factor values for both positions (11.2 and 10.5 Å^2, respectively).

Thr281 is an outlier in the Ramachandran plot of Kleywegt & Jones (1996), with dihedral angle values of $\varphi = 31.7^\circ$ and $\psi = 62.3^\circ$. Both $2F_o - F_c$ and $F_o - F_c$ density maps are featureless for this residue and there is little doubt that its conformation has been assigned correctly. Thr281 is positioned between a 3_{10}-helix (comprising residues 278–280) and Pro282. Its $O^{\gamma 1}$ atom is hydrogen bonded to the O atom of Gly240, as well as to two water molecules (58 and 176). Together, these interactions can explain the slightly unfavourable φ value. It should be noted that the equivalent Thr279 residue in Xyl10A from *S. lividans* (Ducros *et al.*, 2000; PDB code 1e0w) has similar dihedral angle values ($\varphi = 31.4^\circ$ and $\psi = 65.2^\circ$).

A close inspection of the C-terminal end reveals why the glycine-rich tail had been hindering crystal formation and why magnesium in the crystallization reagent had enhanced the process. The last secondary-structure element in the sequence of the crystallized variant is the outer helix α8, comprising residues 293–301. This helix completes and hence closes the barrel. Leu302, the last residue in the sequence, is fixed to the outer wall of the barrel by a hydrogen bond between its OXT atom and the NZ atom of Lys11 and by participating in the octahedral coordination of a magnesium ion (Fig. 4*d*). Five water molecules within 2 Å of the central ion complete the coordination. Any further unstructured extension of the sequence, such as the Gly-rich linker, would protrude from the highly compact catalytic core. As two neighbouring molecules in the crystal are very close to the C-terminal end, a similar packing would have never been attained with the Xys1S form (with the Gly-rich linker).

3.4. Comparison with related xylanase structures

Although Xys1Δ shares the fold common to all family 10 xylanases, some differences can be pinpointed by superimposing it on related structures within the family. We have compared Xys1Δ with the catalytic domain of Xyl10A from *S. lividans* (Ducros *et al.*, 2000; PDB code 1e0w), with the ultrahigh-resolution structure of CTUX from *T. aurantiacus* (Natesh *et al.*, 2003; PDB code 1i1w) and with the structure of Cex from *C. fimi* (White *et al.*, 1994; PDB code 2exo).

The least-squares superposition of these structures, depicted in Fig. 5(*a*), shows that the secondary-structure elements are highly conserved. The r.m.s. deviation of the C^{α}

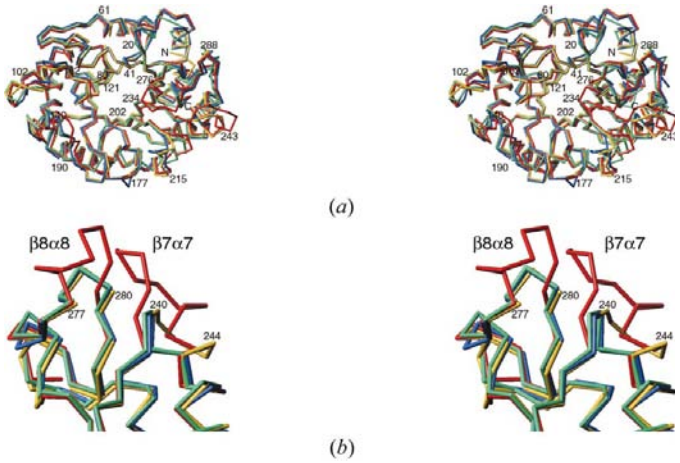

Figure 5
Superimposed C^{α} structures of four family 10 xylanases. (*a*) Top view of the entire catalytic domains. (*b*) Detail of superimposed loops $\beta7\alpha7$ and $\beta8\alpha8$. Labels stand for residue number in the Xys1Δ structure. The displayed traces correspond to xylanase Xys1Δ from *S. halstedii* (yellow), xylanase Xyl10A from *S. lividans* (blue), xylanase 10A from *T. aurantiacus* (green) and Cex from *C. fimi* (red).

atoms after superposition on the Xys1Δ structure is 1.11 Å for Xyl10A (*S. lividans*), 1.42 Å for CTUX (*T. aurantiacus*) and 1.61 Å for Cex (*C. fimi*). Inner β-strands are almost identical in the four structures and only some outer α-helices are slightly displaced. In fact, in a comparison of the structure of the thermostable xylanase from *T. aurantiacus* at two different temperatures, the inner β-barrel is described as a rigid region, whereas the outer helical ring is somewhat flexible (Natesh *et al.*, 2003). This can also be observed in terms of structure conservation when xylanases from different organisms are compared. The $\alpha\beta$-loops of Xys1Δ have nearly the same conformation as those in the other three structures, whereas three of the $\beta\alpha$-loops at the carboxy side of the β-barrel clearly show structural divergences. In fact, the active site is located at the carboxy side of the β-barrel and it is around this region where structural rearrangements will be needed if a different interaction with the substrate has to be fulfilled.

Loop $\beta6\alpha6$ (residues 208–216) of Xys1Δ has the same conformation as in the closely related Xyl10A from *S. lividans* owing to the presence of a proline residue at equivalent positions (212 in *S. halstedii*, 213 in *S. lividans*). In the CTUX and Cex structures lacking the proline residue, the same loop is slightly displaced toward loop $\beta7\alpha7$. The Cex enzyme from *C. fimi* has ten extra residues after strand $\beta7$ when compared with the xylanases from *S. lividans* or *T. aurantiacus* that introduce a completely different structure at loop $\beta7\alpha7$ (Fig. 5*b*). Xys1Δ has three extra residues at the start of helix $\alpha7$ (residues 243–245), which tend to adopt the conformation of the equivalent but longer helical stretch in Cex. The third loop where structural disagreement is obvious is loop $\beta8\alpha8$. In an attempt to introduce a structural subdivision into family 10, two subsets were defined depending on the absence (subset 1) or presence (subset 2) of a helical stretch at loop $\beta8\alpha8$ (Lo Leggio *et al.*, 2001). Xys1Δ is clearly a member of subset 1, as loop $\beta8\alpha8$ does not have the extra helical stretch and is identical to those of xylanases 10A from *S. lividans* and *T. aurantiacus*. On the contrary, the Cex structure has the typical helical extension of subset 2, which might be responsible for the preference for shorter xylooligosacharides compared with subset 1 enzymes (Lo Leggio *et al.*, 2001).

Apart from the aforementioned differences at $\beta\alpha$ loops, which arise mainly from variations in sequence length, the structures of family 10 xylanases are highly conserved. The two glutamic acid residues directly involved in catalysis (Glu127 and Glu235 in Xys1Δ) occupy exactly the same position in the four structures after superposition. The same applies to the surrounding residues at the active site. The two disulfide bonds described here for Xys1Δ are present in the other structures except for the *T. aurantiacus* xylanase, which has a Tyr instead of a Cys residue at position 170 (equivalent to position 168 in *S. halstedii*). The nonprolyl *cis*-peptide bond after the histidine at position 80 (or equivalent) is also a conserved feature.

This study was supported by the Ministerio de Educación y Ciencia (grants PB98-1631, BIO08-0898, BIO2000-1659 and BIO2002-03964) and by the Generalitat de Catalunya (grants 1999SGR188, 2001SGR346 and CERBA). Data collection was supported by the European Union (grants HPRI-CT-1999-00017 and ERBFMGCECT980134 to EMBL Outstation Hamburg).

References

Banner, D. W., Bloomer, A. C., Petsko, G. A., Phillips, D. C., Pogson, C. I., Wilson, I. A., Corran, P. H., Furth, A. J., Milman, J. D., Offord, R. E., Proddle, J. D. & Waley, S. G. (1975). *Nature (London)*, **255**, 609–614.

Brünger, A. T., Adams, P. D., Clore, G. M., DeLano, W. L., Gros, P., Grosse-Kunstleve, R. W., Jiang, J. S., Kuszewski, J., Nilges, M., Pannu, N. S., Read, R. J., Rice, L. M., Simonson, T. & Warren, G. L. (1998). *Acta Cryst.* D**54**, 905–921.

Carson, M. (1997). *Methods Enzymol.* **277**, 493–505.

Collaborative Computational Project, Number 4 (1994). *Acta Cryst.* D**50**, 760–763.

Derewenda, U., Swenson, L., Green, R., Wei, Y., Morosoli, R., Shareck, F., Kluepfel, D. & Derewenda, Z. (1994). *J. Biol. Chem.* **269**, 20811–20814.

Domínguez, R., Souchon, H., Spinelli, S., Dauter, Z., Wilson, K. S., Chavaux, S., Béguin, P. & Alzari, P. M. (1995). *Nature Struct. Biol.* **2**, 569–576.

Ducros, V., Charnock, S. J., Derewenda, U., Derewenda, Z. S., Dauter, Z., Dupont, C., Shareck, F., Morosoli, R., Kluepfel, D. & Davies, G. J. (2000). *J. Biol. Chem.* **275**, 23020–23026.

Evans, P. R. (1993). *Proceedings of the CCP4 Study Weekend. Data Collection and Processing*, edited by L. Sawyer, N. Isaacs & S. Bailey, pp. 114–122. Warrington: Daresbury Laboratory.

Fujimoto, Z., Kuno, A., Kaneko, S., Yoshida, S., Kobayashi, H., Kusakabe, I. & Mizuno, H. (2000). *J. Mol. Biol.* **300**, 575–585.

Harris, G. W., Jenkins, J. A., Connerton, I., Cummings, N., Lo Leggio, L., Scott, M., Hazlewood, G. P., Laurie, J. I., Gilbert, H. J. & Pickersgill, R. W. (1994). *Structure*, **2**, 1107–1116.

Harris, G. W., Jenkins, J. A., Connerton, I. & Pickersgill, R. W. (1996). *Acta Cryst.* D**52**, 393–401.

Henrissat, B. (1991). *Biochem. J.* **280**, 309–316.

Henrissat, B. & Bairoch, A. (1993). *Biochem. J.* **293**, 781–788.

Henrissat, B. & Bairoch, A. (1996). *Biochem. J.* **316**, 695–696.

Henrissat, B. & Davies, G. (1997). *Curr. Opin. Struct. Biol.* **7**, 637–644.
Kabsch, W. & Sander, C. (1983). *Biopolymers*, **22**, 2577–2637.
Kleywegt, G. J. & Jones, T. A. (1996). *Structure*, **4**, 1395–1400.
Laskowski, R., MacArthur, M., Moss, D. & Thornton, J. (1993). *J. Appl. Cryst.* **26**, 283–290.
Lo Leggio, L., Kalogiannis, S., Eckert, K., Teixeira, S. C. M., Bhat, M. K., Andrei, C., Pickersgill, R. W. & Larsen, S. (2001). *FEBS Lett.* **509**, 303–308.
Murshudov, G. N., Lebedev, A., Vagin, A. A., Wilson, K. S. & Dodson, E. J. (1999). *Acta Cryst.* D**55**, 247–255.
Natesh, R., Bhanumoorthy, P., Vithayathil, P. J., Sekar, K., Ramakumar, S. & Viswamitra, M. A. (1999). *J. Mol. Biol.* **288**, 999–1012.
Natesh, R., Manikandan, K., Bhanumoorthy, P., Viswamitra, M. A. & Ramakumar, S. (2003). *Acta Cryst.* D**59**, 105–117.
Navaza, J. (1994). *Acta Cryst.* A**50**, 157–163.
Notenboom, V., Birsan, C., Nitz, M., Rose, D. R., Warren, R. A. J. & Withers, S. G. (1998). *Nature Struct. Biol.* **5**, 812–818.
Otwinowski, Z. (1993). *Proceedings of the CCP4 Study Weekend. Data Collection and Processing*, edited by L. Sawyer, N. Isaacs & S. Bailey, pp. 56–62. Warrington: Daresbury Laboratory.
Perrakis, A., Sixma, T. K., Wilson, K. S. & Lamzin, V. S. (1997). *Acta Cryst.* D**53**, 448–455.
Ramachandran, G. N. & Sasisekharan, V. (1968). *Adv. Protein Chem.* **23**, 283–438.
Roberge, M., Shareck, F., Morosoli, R., Kluepfel, D. & Dupont, C. (1997). *Biochemistry*, **36**, 7769–7775.
Roussel, A. & Cambillau, C. (1989). *Silicon Graphics Partners Directory*, pp. 77–79. Mountain View, CA, USA: Silicon Graphics.
Ruiz-Arribas, A., Fernández-Abalos, J. M., Sánchez, P., Garda, A. L. & Santamaría, R. I. (1995). *Appl. Environ. Microbiol.* **61**, 2414–2419.
Ruiz-Arribas, A., Sánchez, P., Calvete, J. J., Raida, M., Fernández-Abalos, J. M. & Santamaría, R. I. (1997). *Appl. Environ. Microbiol.* **63**, 2983–2988.
Ruiz-Arribas, A., Zhadan, G. G., Kutyshenko, V. P., Santamaría, R. I., Cortijo, M., Villar, E., Fernández-Abalos, J. M., Calvete, J. J. & Shnyrov, V. L. (1998). *Eur. J. Biochem.* **253**, 462–468.
Schmidt, A., Schlacher, A., Steiner, W., Schwab, H. & Kratky, C. (1998). *Protein Sci.* **7**, 2081–2088.
White, A., Tull, D., Johns, K., Withers, S. G. & Rose, D. R. (1996). *Nature Struct. Biol.* **3**, 149–154.
White, A., Withers, S. G., Gilkes, N. R. & Rose, R. R. (1994). *Biochemistry*, **33**, 12546–12552.